

Electronic Supplementary Information (ESI)

**Water-only Hydrothermal Method: a Generalized Route for Environment-benign and Cost-effective Construction of Superhydrophilic Surfaces with Biomimetic Micronanostructures on Metals and Alloys**

**Lingjie Li,<sup>a</sup> Yuezhong Zhang,<sup>a</sup> Jinglei Lei,<sup>\*,a</sup> Jianxin He,<sup>a</sup> Rong Lv,<sup>a</sup> Nianbing Li,<sup>b</sup> and Fusheng Pan<sup>c</sup>**

<sup>a</sup> *School of Chemistry and Chemical Engineering, Chongqing University, Chongqing, 400044, PR China; Fax: +86 23 65112328; Tel.: +86 13983064116; E-mail address:*

*JLLei@cqu.edu.cn;*

<sup>b</sup> *School of Chemistry and Chemical Engineering, Southwest University, Chongqing, 400715, PR China;*

<sup>c</sup> *School of Materials Science and Engineering, Chongqing University, Chongqing, 400044, PR China.*

**S1. Experimental**

Three kinds of metals and alloys, including 2024 Al (composition: 92.81 wt % aluminum, 5.51 wt % copper, and 1.68 wt % magnesium), AZ61 Mg (composition: 92.85 wt % magnesium, 6.20 wt % aluminum, 0.72 wt % zinc, and 0.23 wt % manganese) and pure Cu (99.9 wt % purity) with a working area of 1.0 cm<sup>2</sup> were used as substrates.

The procedures for construction of the superhydrophilic surface with biomimetic micronanostructures are as follows: (1) Pretreatment process for cleaning the surface. The metal plates were abraded with 200, 400, 800# grit emery papers, then degreased ultrasonically in absolute ethanol for 5 min and rinsed with ultrapure water (with the resistance of 18.2 MΩ). (2) Water-only hydrothermal process for constructing the surface micronanostructures. The clean metal plates were promptly introduced into a Teflon-lined stainless steel autoclave that filled with only ultrapure water. The

autoclave was then sealed with a lid and maintained at 120°C for 6 h and subsequently left to cool to room temperature. Then the metal plates were taken out and dried in air.

## **S2. Characterization**

The sample surface morphology was examined by a field emission scanning electron microscope (FESEM, FEI Nova 400, Holland). The chemical composition of the samples was analyzed by X-ray photoelectron spectroscopy (XPS, Thermoelectron ESCALAB250, USA). The phase composition of the samples was identified by X-ray diffractometer (XRD, X'Pert PRO, PANalytical B.V., Holland). The infrared spectra of the samples were investigated by using a Fourier transform infrared spectrometer (FTIR, Nicolet iN10, USA). The surface wettability was evaluated by the water contact angle measurements (CA, Dataphysics OCA20, Germany) under static condition. The average CA value was obtained by more than five valid measurements on different spots of the same sample.

## **S3. Results and discussion**

### *S3.1 2024 Al sample*

The XPS results of the untreated 2024 Al surface are presented in Fig. S1. Fig. S1a and S1b respectively show the high-resolution spectra of Al 2*p* and O 1*s*. The Al 2*p* spectrum can be fitted by two peaks, centered at 74.4 eV and 72.7 eV, respectively assigning to native oxide (Al<sub>2</sub>O<sub>3</sub>) and Al.<sup>1</sup> The O 1*s* spectrum can be decomposed into two peaks at 532.2 eV and 529.9 eV, respectively attributing to O element contaminated with air and in Al<sub>2</sub>O<sub>3</sub>.<sup>2</sup> The untreated 2024 Al surface is thus inferred to cover with a native oxide film.

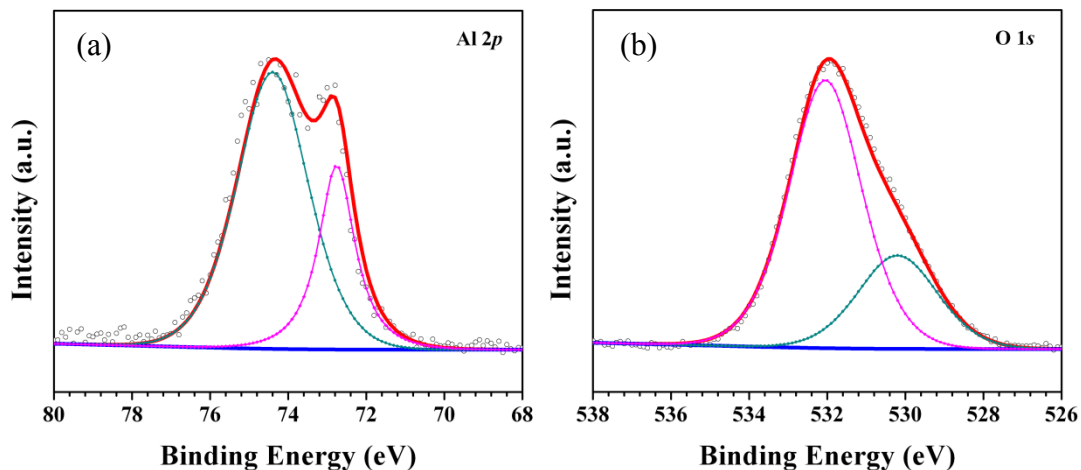


Fig. S1 XPS ( $Al K\alpha$ ) spectra of untreated 2024 Al sample: (a) Al  $2p$  high-resolution spectrum and (b) O  $1s$  high-resolution spectrum.

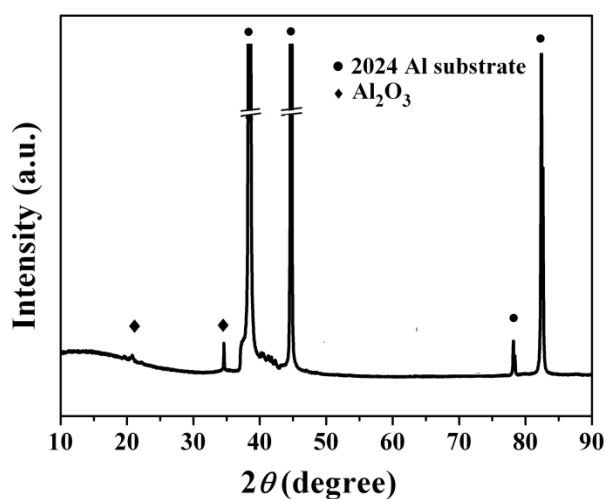


Fig. S2 XRD patterns of untreated 2024 Al sample

Fig. S2 illustrates the XRD patterns of the untreated 2024 Al sample. Besides the strong diffraction peaks of 2024 Al substrate, the featured diffraction peaks for  $Al_2O_3$  are observed,<sup>3</sup> which confirms the former XPS results that the untreated 2024 Al surface is covered with a thin film of native oxide.

Fig. S3 shows the survey XPS spectrum of 2024 Al sample after the water-only hydrothermal process. It indicates that only Al, O and C exist on the sample surface,

among which C is contamination induced during storage of the sample in air.

Fig. S4 illustrates the XRD patterns of 2024 Al sample after the water-only hydrothermal process. Besides the strong diffraction peaks of 2024 Al substrate, the obvious diffraction peaks of aluminum oxyhydroxide - boehmite ( $\text{AlOOH}$ ), alumina ( $\text{Al}_2\text{O}_3$ )<sup>3</sup> are observed, which confirms the former XPS results that the 2024 Al surface after the water-only hydrothermal treatment consists of  $\text{AlOOH}$  and  $\text{Al}_2\text{O}_3$ .

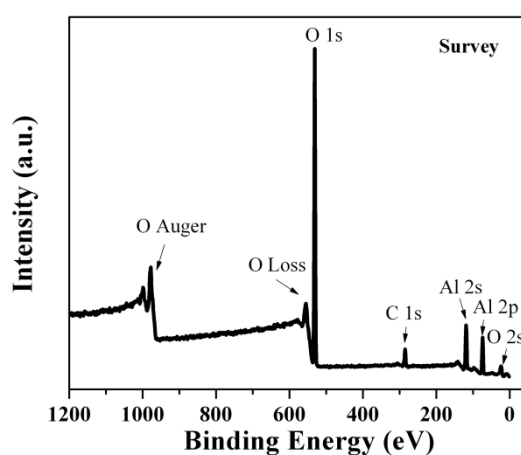


Fig. S3 XPS ( $\text{Al } K\alpha$ ) survey spectrum of 2024 Al sample after water-only hydrothermal process.

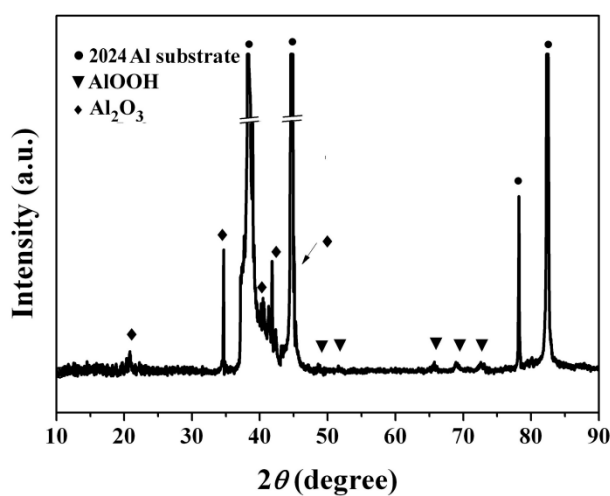


Fig. S4 XRD patterns of 2024 Al sample after water-only hydrothermal process.

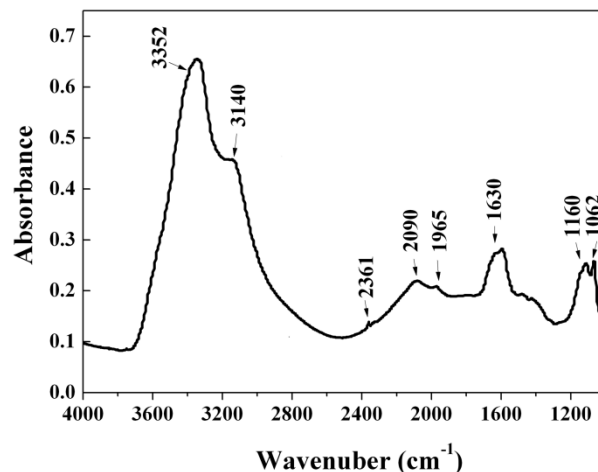


Fig. S5 FTIR spectrum of 2024 Al sample after water-only hydrothermal process.

Fig. S5 shows the FTIR result of 2024 Al sample after the water-only hydrothermal treatment. The intensive bands at 3352  $\text{cm}^{-1}$  and 3140  $\text{cm}^{-1}$  can be respectively assigned to the  $\nu_{\text{as}}(\text{Al})\text{O-H}$  and  $\nu_{\text{s}}(\text{Al})\text{O-H}$  stretching vibrations.<sup>3</sup> The intensive band at 1062  $\text{cm}^{-1}$  and the shoulder at 1160  $\text{cm}^{-1}$  are respectively attributed to the  $\delta_{\text{s}} \text{Al-O-H}$  and  $\delta_{\text{as}} \text{Al-O-H}$ .<sup>4</sup> The two weak bands at 2090  $\text{cm}^{-1}$  and 1965  $\text{cm}^{-1}$  are the combination bands.<sup>4,5</sup> The weak band at 1630  $\text{cm}^{-1}$  can be assigned to the stretching and bending modes of the adsorbed water.<sup>5</sup> In addition, the band at 2361  $\text{cm}^{-1}$  can be ascribed to the adsorbed  $\text{CO}_2$ .<sup>6</sup>

### S3.2 AZ61 Mg sample

Fig. S6 illustrates the water droplet (2  $\mu\text{L}$ ) shape on untreated clean AZ61 Mg surface, which shows a water contact angle of ca. 83°, indicating the hydrophilic nature of the alloy surface.

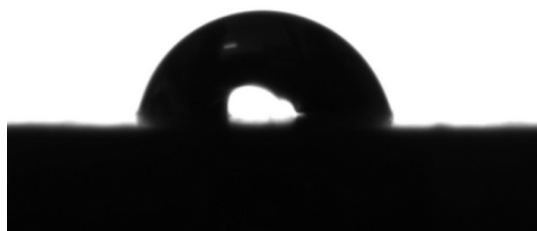


Fig.S6 Digital photograph of water droplet (2  $\mu\text{L}$ ) shape on untreated clean AZ61 Mg surface.

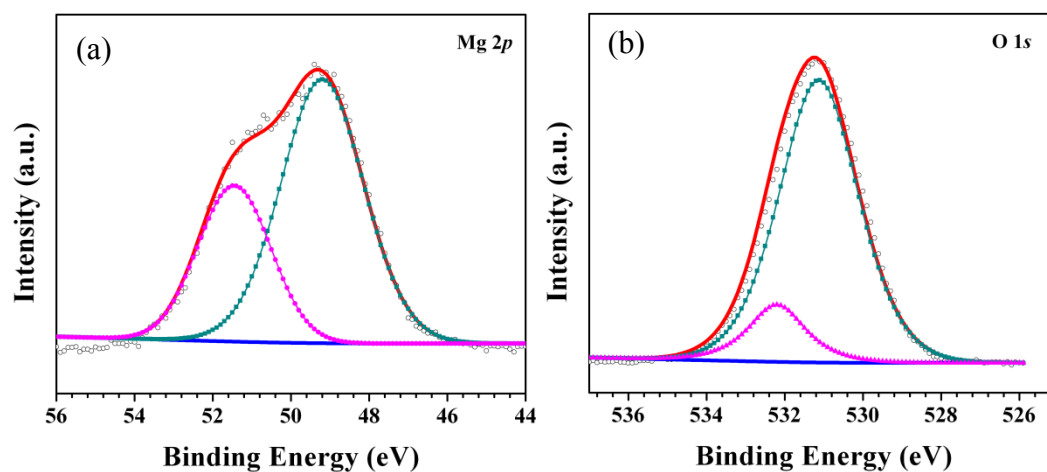


Fig. S7 XPS ( $\text{Al } K\alpha$ ) spectra of untreated AZ61 Mg sample: (a) Mg 2p high-resolution spectrum and (b) O 1s high-resolution spectrum.

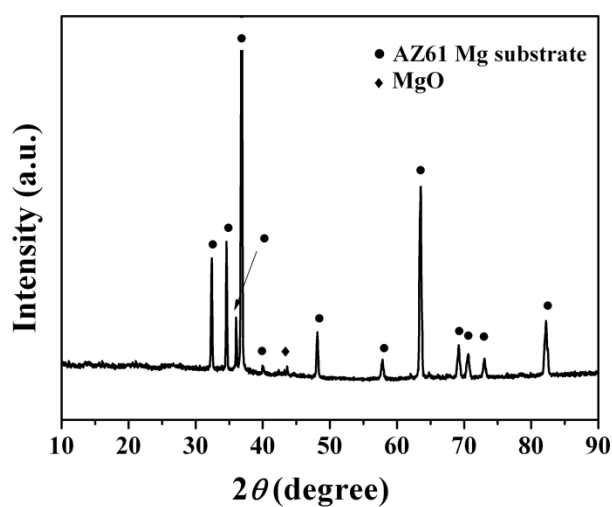


Fig. S8 XRD patterns of untreated AZ61 Mg sample

The XPS results of the untreated AZ61 Mg surface are presented in Fig. S7. Fig. S7a and S7b respectively show the high-resolution spectra of Mg  $2p$  and O  $1s$ . The Mg  $2p$  spectrum displays two peaks, which are centered at 51.5 eV and 49.2 eV, respectively assigning to native oxide (MgO) and Mg.<sup>1</sup> The O  $1s$  spectrum can be decomposed into two peaks at 532.2 eV and 531.6 eV, respectively attributing to O element contaminated with air and in MgO.<sup>7,8</sup> The untreated AZ61 Mg surface is thus inferred to cover with a native oxide film.

Fig. S8 illustrates the XRD patterns of the untreated AZ61 Mg sample. Besides the strong diffraction peaks of AZ61 Mg substrate, the weak diffraction peaks for MgO are present,<sup>9</sup> which confirms the former XPS results that the untreated AZ61 Mg surface is covered with a thin film of native oxide.

The XPS results of AZ61 Mg surface after the water-only hydrothermal treatment are presented in Fig. S9. The survey XPS spectrum (Fig. S9a) indicates that Mg, O, and C elements mainly exist at the surface, among which C is contamination induced during storage of the sample in air. Fig. S9b and S9c respectively show the high-resolution spectra of Mg  $2p$  and O  $1s$ . The Mg  $2p$  spectrum displays two peaks, which are centered at 51.9 eV and 49.6 eV, assigning to Mg(OH)<sub>2</sub> and MgO, respectively.<sup>7</sup> The O  $1s$  spectrum can be decomposed into two peaks at 531.6 eV and 532.7 eV, attributing to O element in MgO and Mg(OH)<sub>2</sub>, respectively.<sup>8</sup> The AZ61 Mg surface after the water-only hydrothermal treatment is thus inferred to mainly consist of MgO and Mg(OH)<sub>2</sub>.

Fig. S10 illustrates the XRD patterns of AZ61 Mg sample after the water-only hydrothermal process. Besides the strong diffraction peaks of AZ61 Mg substrate, the diffraction peaks of magnesia (MgO),<sup>9</sup> magnesium hydroxide [Mg(OH)<sub>2</sub>]<sup>10</sup> are present, which confirms the former XPS results that the AZ61 Mg surface after the water-only hydrothermal treatment mainly consists of MgO and Mg(OH)<sub>2</sub>.

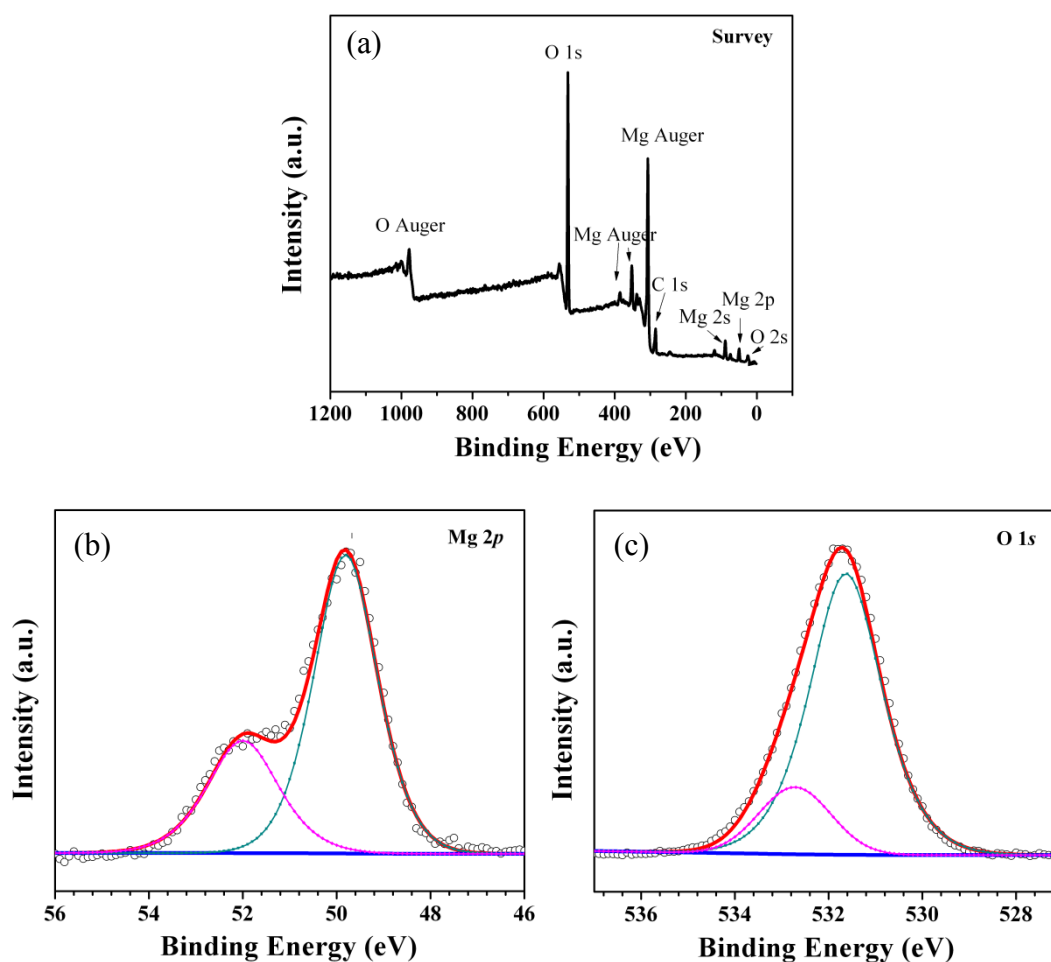


Fig. S9 XPS (Al  $K\alpha$ ) spectra of AZ61 Mg sample after water-only hydrothermal process: (a) survey spectrum, (b) Mg 2p high-resolution spectrum and (c) O 1s high-resolution spectrum.

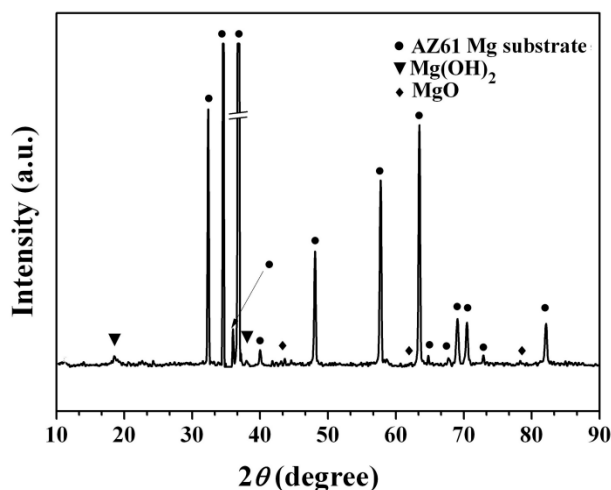


Fig. S10 XRD patterns of AZ61 Mg sample after water-only hydrothermal process.

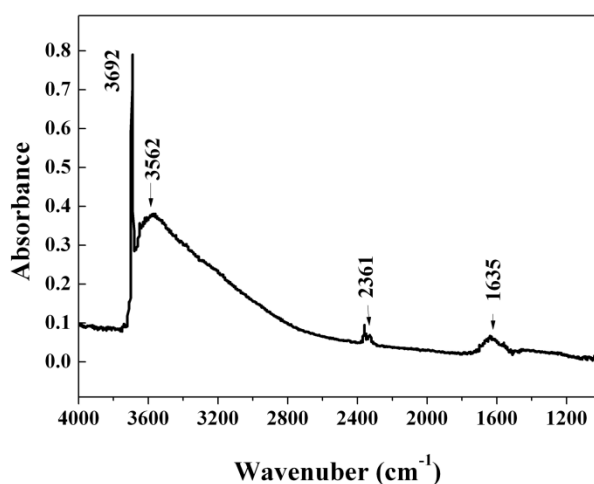


Fig. S11 FTIR spectrum of AZ61 Mg sample after water-only hydrothermal process.

Fig. S11 shows the FTIR result of AZ61 Mg sample after the water-only hydrothermal treatment. The intensive bands at  $3692\text{ cm}^{-1}$  and  $3562\text{ cm}^{-1}$  can be assigned to the (Mg)O–H and O–H stretching vibrations.<sup>10</sup> The weak band at  $1635\text{ cm}^{-1}$  can be ascribed to the stretching and bending modes of the adsorbed water.<sup>5</sup> The band at  $2361\text{ cm}^{-1}$  can be attributed to the adsorbed  $\text{CO}_2$ .<sup>6</sup>

### S3.3 Pure Cu sample

Fig. S12 illustrates the water droplet ( $2\text{ }\mu\text{L}$ ) shape on untreated clean Cu surface,

which shows a water contact angle of ca.  $62^\circ$ , indicating the hydrophilic nature of the pure Cu surface.



Fig. S12 Digital photograph of water droplet ( $2\ \mu\text{L}$ ) shape on untreated clean Cu surface.

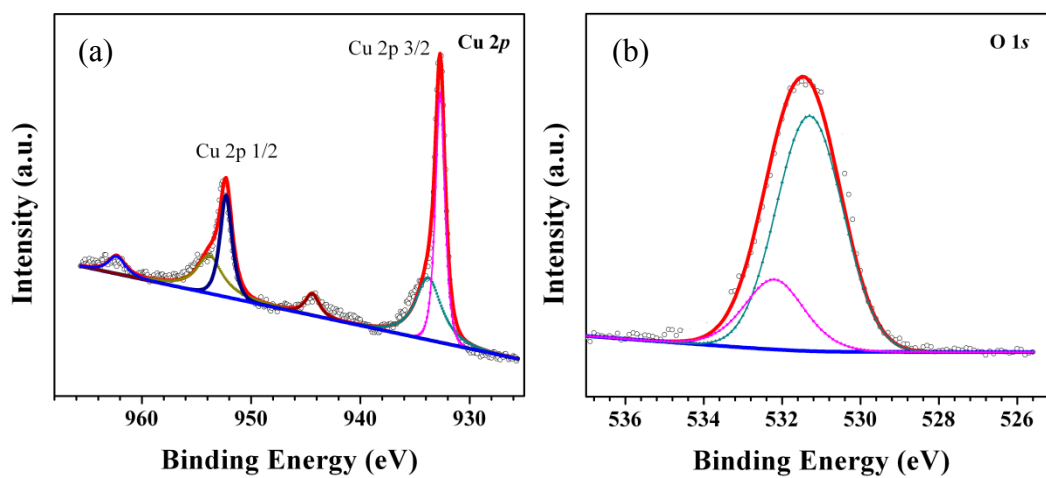


Fig.S13 XPS ( $\text{Al } K\alpha$ ) spectra of untreated Cu sample: (a) Cu 2p high-resolution spectrum and (b) O 1s high-resolution spectrum.

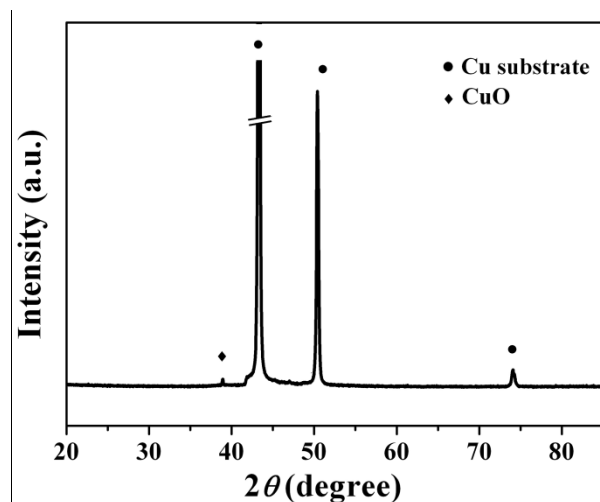


Fig. S14 XRD patterns of untreated Cu sample.

The XPS results of the untreated Cu surface are presented in Fig. S13. Fig.S13a and S13b respectively show the high-resolution spectra of Cu  $2p$  and O  $1s$ . The Cu  $2p_{3/2}$  peaks centered at 931.8 and 933.7 eV, and the Cu  $2p_{1/2}$  peaks centered at 951.8 eV and 953.6 eV, are accompanied with the corresponding characteristic satellite peaks at 943.5 eV and 962.5 eV, attributing to Cu (0) and Cu (+2) states.<sup>1,11</sup> The O  $1s$  spectrum can be decomposed into two peaks at 532.2 eV and 530.6 eV, respectively attributing to O element contaminated with air and in CuO.<sup>11</sup> The untreated Cu surface is thus inferred to cover with a native oxide film.

Fig. S14 illustrates the XRD patterns of the untreated Cu sample. Besides the strong diffraction peaks of Cu substrate, the weak diffraction peak for CuO is present,<sup>11</sup> which confirms the former XPS results that the untreated Cu surface is covered with a thin film of native oxide.

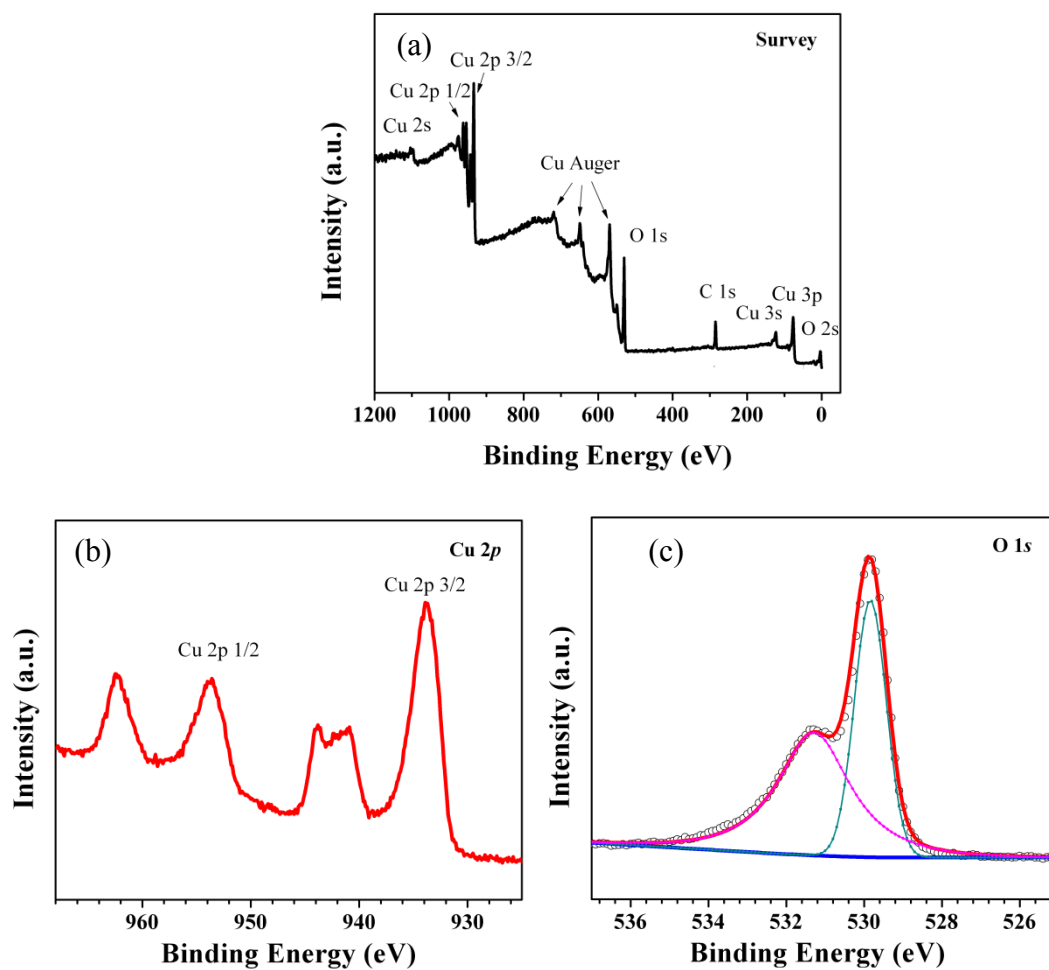


Fig. S15 XPS ( $Al K\alpha$ ) spectra of Cu sample after water-only hydrothermal process: (a) survey spectrum, (b) Cu  $2p$  high-resolution spectrum, (c) O  $1s$  high-resolution spectrum

The XPS results of Cu surface after the water-only hydrothermal treatment are presented in Fig. S15. The survey XPS spectrum (Fig. S15a) indicates that only Cu, O, and C exist at the surface, among which C is contamination induced during storage of the sample in air. Fig. S15b and S15c respectively show the high-resolution spectra of Cu  $2p$  and O  $1s$ . The Cu  $2p_{3/2}$  and  $2p_{1/2}$  peaks are respectively centered at 933.7 eV and 953.6 eV, which are accompanied with the corresponding characteristic satellite peaks at 943.5 eV and 962.5 eV, attributing to a Cu(+2) state in  $Cu(OH)_2$  and  $CuO$ .<sup>11</sup>

<sup>12</sup> The O 1s spectrum can be decomposed into two peaks at 531.3 eV and 529.9 eV, attributing to O element in Cu(OH)<sub>2</sub> and CuO, respectively.<sup>12</sup> The Cu surface after the water-only hydrothermal treatment is thus inferred to essentially consist of CuO and Cu(OH)<sub>2</sub>.

The XRD patterns of Cu sample after the water-only hydrothermal process are illustrated in Fig. S16. Besides the strong diffraction peaks of pure Cu substrate, the diffraction peaks of copper hydroxide [Cu(OH)<sub>2</sub>],<sup>11</sup> copper oxide (CuO)<sup>12</sup> are observed, which confirms the former XPS results that the Cu surface after the water-only hydrothermal treatment consists of CuO and Cu(OH)<sub>2</sub>.

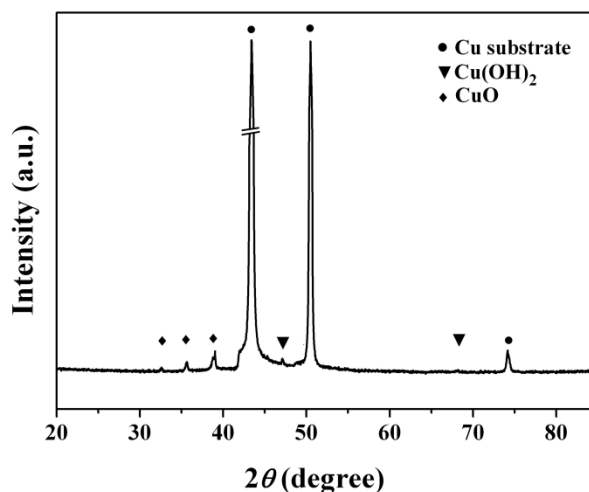


Fig. S16 XRD patterns of Cu sample after water-only hydrothermal process.

Fig. S17 shows the FTIR result of Cu sample after the water-only hydrothermal treatment. The bands at 3573 cm<sup>-1</sup> and 3440 cm<sup>-1</sup> can be assigned to (Cu)O–H and O–H stretching vibrations.<sup>13,14</sup> The band at 1631 cm<sup>-1</sup> can be ascribed to the stretching vibration and bending vibration of the absorbed water.<sup>5,13</sup> Additionally, the band at 2361 cm<sup>-1</sup> can be attributed to the adsorbed CO<sub>2</sub>.<sup>6</sup>

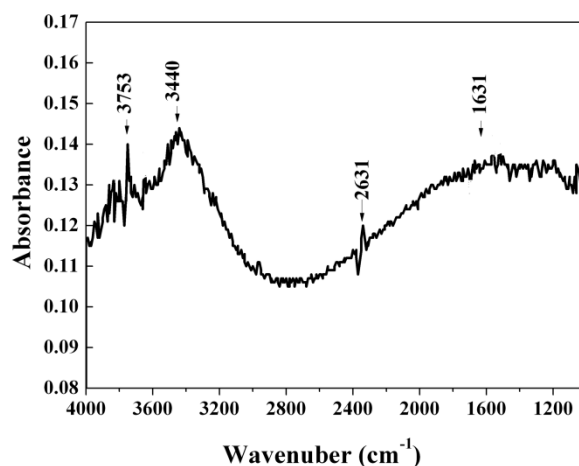


Fig. S17 FTIR spectrum of Cu sample after water-only hydrothermal process.

### References:

- [1]C. D. Wagner, J. F. Moulder, J. E. Davis and W. M. Riggs, Handbook of X-ray Photoelectron Spectroscopy, Perkin-Elmer Corp., Eden Prairie, MN, USA, 1992, pp. 53, 55, 87.
- [2] V. Vignal, H. Krawiec, O. Heintz and D. Mainy, *Corros. Sci.*, 2013, **67**, 109-117.
- [3]L. M. Zhang, W. C. Lu, R. R. Cui and S. S. Shen, *Mater. Res. Bull.* 2010, **45**, 429-436.
- [4]G. J. Ji, M. M. Li, G. H. Li, G. M. Gao, H. F. Zou, S. C. Gan and X. C. Xu, *Powder Technol.* 2012, **215-216**, 54-58.
- [5]H. W. Hou, Y. Xie, Q. Yang, Q. X. Guo and C. R. Tan, *Nanotechnology*, 2005, **16**,741-745.
- [6]A. Zukal, C. O. Arean, M. R. Delgado, P. Nachtigall, A. Pulido, J. Mayerova and J. Cejka, *Microporous Mesoporous Mater.*,2011, **146**, 97-105.

- [7]M. Liu, P. Schmutz, S. Zanna, A. Seyeux, H. Ardelean, G. L. Song, A. Atrens and P. Marcus, *Corros.Sci.*, 2010, **52**, 562-578.
- [8]M. Liu, S. Zanna, H. Ardelean, I. Frateur, P. Schmutz, G. L. Song, A. Atrens and P. Marcus, *Corros.Sci.*,2009, **51**, 1115-1127.
- [9]J. Scholz, A. Walter, A. H. P. Hahn and T. Ressler, *Microporous Mesoporous Mater.*, 2013, **180**, 130-140.
- [10]T. Ishizaki, S. Chiba, K. Watanabe and H. Suzuki, *J. Mater. Chem. A*, 2013,**1**, 8968-8977.
- [11]M. Basu, A. K. Sinha, M. Pradhan, S. Sarkar, Y. Negishi and T. Pal, *J. Phys. Chem. C*, 2011, **115**, 20953-20963.
- [12] A. Chaudhary and H. C. Barshilia, *J. Phys. Chem. C*, 2011, **115**, 18213-18220.
- [13]C. F. Li, Y. D. Yin, H. G. Hou, N. Y. Fan, F. L. Yuan, Y. M. Shi and Q. L. Meng, *Solid State Commu.*, 2010, **150**, 585-589.
- [14]Z. Sun, Y. Sun, Q. H. Yang, X. J. Wang and Z. H. Zheng, *Surf. Coat. Technol.*, 1996, **79**, 108-112.